International Journal of Plasticity 164 (2023) 103574

Contents lists available at ScienceDirect

International Journal of Plasticity

journal homepage: www.elsevier.com/locate/ijplas

The optimum grain size for strength-ductility combination in metals

Yanfei Wang [a], Chongxiang Huang [b], Xiaolong Ma [c], Jianfeng Zhao [d], Fengjiao Guo [b], Xiaotian Fang [e], Yuntian Zhu [c,*], Yueguang Wei [a,*]

[a] Department of Mechanics and Engineering Science, College of Engineering, Peking University, Beijing 100871, China
[b] School of Aeronautics and Astronautics, Sichuan University, Chengdu 610065, China
[c] Department of Materials Science and Engineering, City University of Hong Kong, Hong Kong, China
[d] Institute of Systems Engineering, Chinese Academy of Engineering Physics, Mianyang 621999, China
[e] Department of Materials Science and Engineering, North Carolina State University, Raleigh, NC 27695, USA

ARTICLE INFO

Keywords:
Strength and ductility
Grain size effect
Grain boundary affected region
Geometrically necessary dislocations
Heterostructure

ABSTRACT

A strength-ductility trade-off usually occurs when grains are refined to increase strength. A question arises on if there exists a grain size for the best strength-ductility combination, i.e., with the highest possible strain energy density limit and strength simultaneously. This issue is crucial for guiding the design of strong and tough structural materials. Here we reveal an optimum grain size ($d_{optimum}$) on the order of a few micrometers, at which the strain energy density limit, estimated as the product of strength and uniform elongation, reaches a maximum while maintaining reasonably high yield strength. The $d_{optimum}$ is found to exist in a series of single-phase FCC, BCC and HCP materials, indicating it as a universal phenomenon. Theoretical models on the grain size-dependence of uniform elongation and ultimate strength are developed by considering dislocation accumulation in grain boundary affected region (Gbar) and grain interior based on the classical Kocks-Mecking-Estrin model. Combined with the Hall-Petch relationship, the models accurately predict the $d_{optimum}$. Importantly, the models disclose this $d_{optimum}$ to be close to twice of the characteristic width of Gbar (l_{Gbar}), suggesting that it is exactly at or near the critical grain size with the strongest intragranular strain gradient effects.

1. Introduction

Metallic materials are desired to be strong and ductile at the same time. Unfortunately, these two properties are usually mutually exclusive, especially when manipulating grain size (d) to improve one of them (Meyers et al., 2006). Good ductility originates from high work hardening capability, which helps to resist strain localization and consequently prevent catastrophic failure (Ritchie, 2011; Zhu and Wu, 2018). This is one of the key reasons why coarse-grained (CG) materials remain the primary choice for most structural applications. However, the low strength of CG material requires more materials to carry the load, which makes it less energy efficient in applications (Li and Lu, 2017). Grain refinement can effectively strengthen materials, but it usually sacrifices ductility. As extreme cases, ultrafine-grained (UFG) and nanostructured (NS) materials can be many times stronger than their CG counterparts, but their ductility is typically lower than 5% (Lu, 2014; Ovid'ko et al., 2018). This presents a major problem for the high-strength NS bulk to

* Corresponding author.
E-mail addresses: y.zhu@cityu.edu.hk (Y. Zhu), weiyg@pku.edu.cn (Y. Wei).

https://doi.org/10.1016/j.ijplas.2023.103574
Received 7 December 2022; Received in revised form 14 February 2023;
Available online 27 February 2023

serve in safety-critical applications. Such grain size-related strength-ductility trade-off raises a few critical issues. Does an optimum grain size ($d_{optimum}$) exist for strength-ductility combination? If so, how to determine and predict the $d_{optimum}$ theoretically? Furthermore, what is the mechanism behind it?

These issues are not only fundamental to understanding the grain size effects on mechanical behavior, but also important for guiding the microstructural design of high-performance materials, including the conventional engineering materials and advanced composites. For example, in the heterostructured materials, superior strength-ductility combination is expected if the grain size of the heterogeneous constituent zones can be tuned to the corresponding $d_{optimum}$ (Sathiyamoorthi and Kim, 2020; Zhu et al., 2021). Despite the relentless efforts in optimizing strength-ductility combination by largely manipulating the microstructures (Li and Lu, 2017; Wu et al., 2022, 2015; Zhong et al., 2022), the chemistry (Li et al., 2016; L. Y. Liu et al., 2022), or both at the same time (Fan et al., 2022; S. S. Liu et al., 2022), the present issues remain unsettled in theoretical understanding.

Achieving the best strength-ductility combination generally means that at the highest possible strength level, the strain energy density limit reaches or approaches the maximum. The difficulty in predicting the $d_{optimum}$ lies in the complexity of grain size effects on the strength and ductility that govern the strain energy density limit. Although the yield strength can be simply evaluated using the Hall-Petch equation (Hansen, 2004; Meyers and Chawla, 2009), the dependence of ductility and ultimate strength on grain size are not well understood (Li and Cui, 2007). Since ductility and ultimate strength are deformation history-dependent properties governed by work hardening and plastic instability (Yasnikov et al., 2022; Zhu and Wu, 2018), their dependence on grain size is primarily due to the interaction between dislocations and grain boundary. At the plastic stage, grain boundaries act as extra barriers to block dislocation motion and sites for dynamic recovery, resulting in distinct dislocation accumulations in the vicinity of grain boundary and in the grain interior (Delincé et al., 2007; Haouala et al., 2018; Hirth, 1972; Meyersm and Ashworth, 1982). Along with these behaviors, significant intragranular strain inhomogeneity is developed, which complicates the distribution of both short- and long-range internal stresses within grains (Ashby, 1970; Jiang et al., 2022). Grain refinement embraces more extensive grain boundary-dislocation interactions. As extreme cases, when the grain size is reduced to ultrafine or nanometer scale, the free slip path and storage room of dislocations are largely limited by the high-density grain boundaries, and the dynamic recovery is gradually dominated by grain boundaries (Meyers et al., 2006; Yu et al., 2005). The coupling of these factors complicates the interpretation of grain size effects on work hardening, making it a great challenge to derive explicit models on the grain size dependence of ductility and ultimate strength, and thus obscuring the reasoning path towards $d_{optimum}$.

Nevertheless, some recent experimental results may provide a potential hint on the possible $d_{optimum}$. Specifically, fine grains (FG) of a few micrometers were coincidentally involved in a variety of advanced structures with superior strength-ductility combination, including in homogeneous materials (Guo et al., 2022; Li et al., 2008; M.W. Liu et al., 2022; M.S. Wang et al., 2022), heterostructured materials (Huang et al., 2018; Wang et al., 2002; Wu et al., 2015), and conventional composites (Wu et al., 2017). For instance, in partially recrystallized Ti and Cu, both of which unite the UFG strength and the CG ductility, the FG zones with a grain size of about 2–4 μm were believed to play the key role in retaining work hardening (Wang et al., 2002; Wu et al., 2015). In the recently designed strong-yet-ductile manganese steel and complex-concentrated Ni-Fe alloys, FGs were the main constituent (Fan et al., 2022; Zhong et al., 2022). There appears to be some kinds of efficient strengthening and hardening mechanisms in this size range. Unfortunately, most of these structures were designed by trial and error, lacking clear physical guidelines on the grain size. In short, the confirmation of the existence and the exact value of $d_{optimum}$ as well as the possible deformation physics behind it remain elusive.

In this work, experimental results on the tensile properties of a series of single-phase materials with various crystal structures are collected over a wide grain size range, from extensive literature available to the authors. Systematic analyses on grain size effects verify that there indeed exists universally a $d_{optimum}$ at which the optimal strength-ductility combination is achieved. Theoretical models on grain size effects are established to predict the $d_{optimum}$. Deformation physics potentially responsible for the superior properties at $d_{optimum}$ will be discussed. Note that the $d_{optimum}$ is currently discussed in terms of the quasi-static tension properties at ambient temperature, with dislocation-dominated plasticity, in order to deliver more general fundamentals.

2. Experimental data collection

In the literature and practice, ductility has been defined as the uniform elongation or the elongation to failure (Ovid'ko et al., 2018). Uniform elongation is generally less affected by the gage dimension of specimen. In contrast, the high dependence of necking strain on gage length often makes the elongation to failure artificially high or even meaningless if the uniform segment is relatively low and/or non-standard small specimen is used (Zhu and Wu, 2018), such as in the tests commonly carried for UFG/NS materials. For this reason, uniform elongation was advised to be more suitable as a measure of ductility (Ovid'ko et al., 2018; Zhu and Wu, 2018), which is also the case of present research. The yield strength (σ_y), ultimate strength (σ_{uts}), uniform elongation (δ_u) and grain size (d) of a series of single-phase materials are collected from literature based on the following principles. First, to ensure the comparability of data from different papers, the experimental test must be standard quasi-static uniaxial tension at room temperature using bulk samples, and the purity or chemical composition of material is strictly regulated. For instance, the purity of Cu is required to be >99.9%. Second, to ensure reliability, the data accompanied by well-defined stress-strain curves are highly preferred. Some stress-strain curves in literature have extremely low elastic modulus due to machine compliance, which are elaborately normalized with respect to the theoretical modulus before data analysis. Third, only materials with homogeneous microstructures are considered. Fourth, twin boundaries are treated as grain boundaries in grain size statistics.

The grain size range considered is typically from ~0.1 μm to ~100 μm, within which plastic deformation is largely dominated by dislocation-based mechanisms. Except for the NS materials ($d < 0.5$ μm generally) processed by severe plastic deformation, all other

materials have a fully recrystallized (RX) uniform microstructure. The recrystallized materials with grain size in the range of 0.1∼1 μm, 1∼5 μm and >5 μm are hereinafter referred to as RX UFG, RX FG and RX CG, respectively. The strain hardening exponent is derived from the linear regression of five points taken from the true $\log\varepsilon - \log\sigma$ curve in geometrical progression within $0.2\delta_u$-$0.8\delta_u$, following the ASTM standard E646.

3. Results

3.1. The optimum grain size ($d_{optimum}$) for strength-ductility combination

We first take pure Cu as an example to probe the effect of grain size on mechanical properties. As shown in Fig. 1, the NS Cu displays high yield strength (>350 MPa) but poor ductility. Recrystallization leads to a rapid recovery of ductility in the FG regime (Fig. 1*A*), whereas the yield strength decreases gradually but still remains at a reasonably high level (300–100 MPa, Fig. 1*B*). The uniform elongation increases to almost 30% when grain size approaches 5 μm, at which the yield strength is ∼100 MPa. Further grain growth by annealing is accompanied by a rapid level-off of ductility. At the same time, the decrease in yield strength slows down upon entering the CG regime. These observations indicate a reduced grain size effect in the CG regime. The ultimate strength evolves with grain size in a way similar to that of yield strength.

As shown, the mutually exclusive of strength and ductility makes it difficult to identify the optimal combination. A combination of high strength and high ductility means that the material has high strain energy density limit under tension, i.e., great energy dissipation capability without fracturing, which can also be understood as having high tension toughness before necking (Ritchie, 2011;

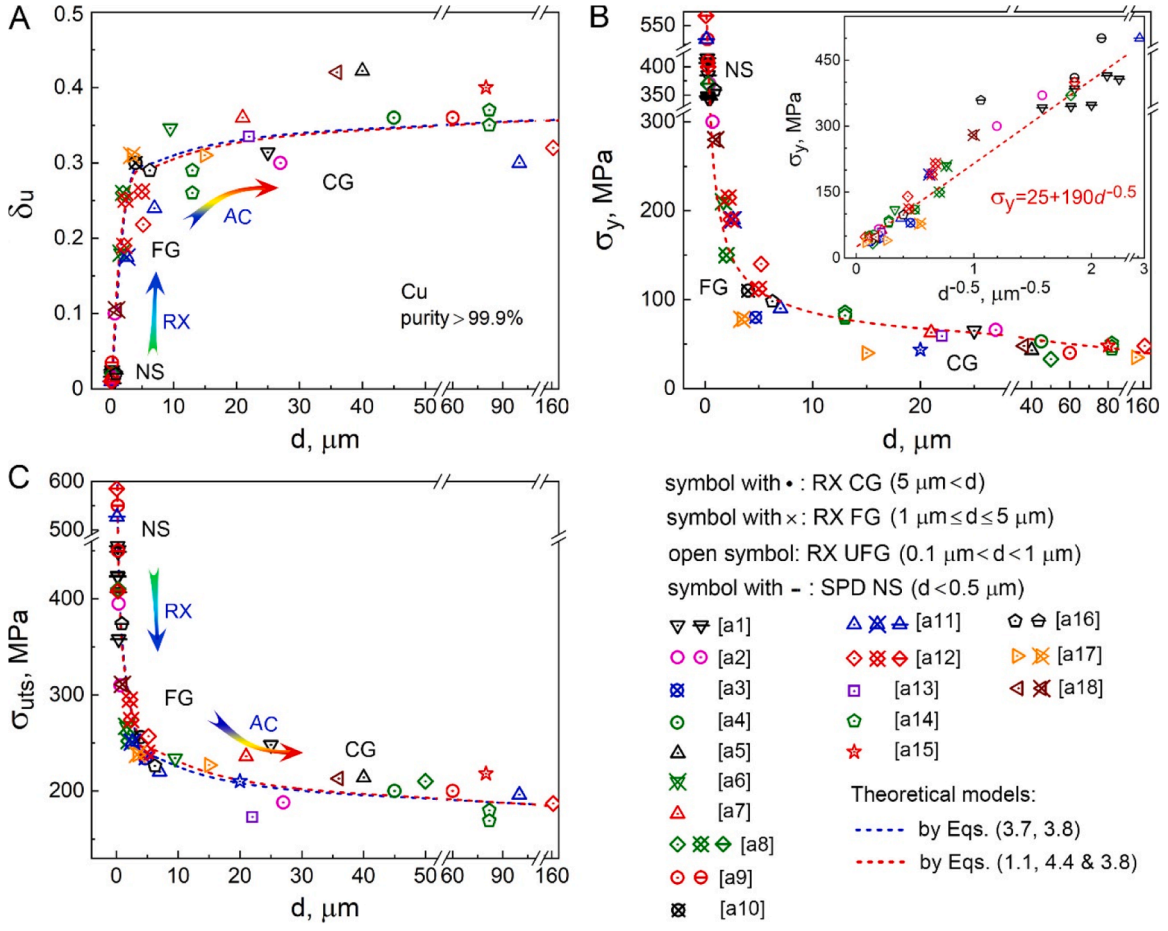

Fig. 1. The variation of (A) δ_u, (B) σ_y and (C) σ_{uts} as a function of grain size d in pure Cu. The dotted lines are the numerical result of theoretical models, which will be derived in Section 4. AC represents annealing coarsening, and SPD represents severe plastic deformation. Experimental data are collected from the following literatures: a1 (Dalla Torre et al., 2004), a2 (Xue et al., 2012), a3 (Ren et al., 2018), a4 (Yang et al., 2015), a5 (Wang et al., 2019a), a6 (Mazaheri et al., 2021), a7 (Fang et al., 2011), a8 (Zhao et al., 2011), a9 (Zhao et al., 2006), a10 (Ma et al., 2015), a11 (An et al., 2012), a12 (Li et al., 2008), a13 (Ebrahimi et al., 1998), a14 (Yang and Lu, 2013), a15 (Liu et al., 2016), a16 (Wang et al., 2019b), a17 (Thompson and Baskes, 1973), a18 (Wang et al., 2018a). (For interpretation of the references to color in this figure legend, the reader is referred to the web version of this article.)

Sih and Macdonald, 1974; Soboyejo, 2003). Therefore, the product of strength and ductility, essentially an approximation of strain energy density limit or tension toughness, can be used as the index to evaluate the strength-ductility combination (Pan et al., 2021; Soboyejo, 2003). Here two indexes can be used: the product of ductility and the average of yield strength and ultimate strength, $\delta_u*(\sigma_y+\sigma_{uts})/2$, and the product of ductility and yield strength, $\delta_u*\sigma_y$. The former actually fits the area enclosed by the ascending branch of tensile engineering stress-strain curve, representing a more accurate approximation of strain energy density limit, whereas the latter is more convenient for engineering practice and can manifest the superiority of the material with moderate ductility but high yield strength.

Figs. 2*A-B* show the variation of $\delta_u*(\sigma_y+\sigma_{uts})/2$ and $\delta_u*\sigma_y$ as a function of grain size. The poor ductility of high-strength NS materials renders them extremely low values. Interestingly, recrystallization leads to a quick improvement in both $\delta_u*(\sigma_y+\sigma_{uts})/2$ and $\delta_u*\sigma_y$, which simultaneously peak in the FG regime near a critical grain size of d_c~2.5 μm, and then decrease gradually with further increasing grain size in the CG regime. The appearance of prominent peaks suggests that the toughest under tension is actually the FG material, rather than its CG counterpart what we usually think of as tough material. The $\delta_u*(\sigma_y+\sigma_{uts})/2$ and $\delta_u*\sigma_y$ are plotted versus yield strength in Figs. 2*C-D*. As shown, the FG with size near d_c (symbols with ×) is about 2–5 times stronger than CG. The $\delta_u*(\sigma_y+\sigma_{uts})/2$ and $\delta_u*\sigma_y$ drop dramatically if strength higher than that of FG is pursued. These reveal that the material is initially toughened and strengthened simultaneously as grain size gradually decreases, but further strengthening after reaching d_c is at the expense of strain energy density limit. In other words, at the d_c the maximum of strain energy density limit is attained with a rather high strength, which is exactly what is meant by the best strength-ductility combination. Therefore, the d_c is exactly the $d_{optimum}$.

These findings firmly substantiate several fundamentals, at least for pure Cu. First, the $d_{optimum}$ for strength-ductility combination does exist. Second, the $d_{optimum}$ is on the order of a few micrometers, falling into the FG regime. Third, the $d_{optimum}$ is essentially the limiting dimension that allows toughening by grain refinement, at which the strain energy density limit reaches a maximum while maintaining fairly high yield strength. Note that the $d_{optimum}$ revealed by the two indexes are in perfect consistency, further verifying their validity.

3.2. *Universality of the* $d_{optimum}$

To probe whether the existence of $d_{optimum}$ is universal, we further examined the variation of $\delta_u*(\sigma_y+\sigma_{uts})/2$ and $\delta_u*\sigma_y$ with grain size in more materials with different crystal structures and properties, including the bcc interstitial free (IF) steel (Fig. 3), hcp pure Ti

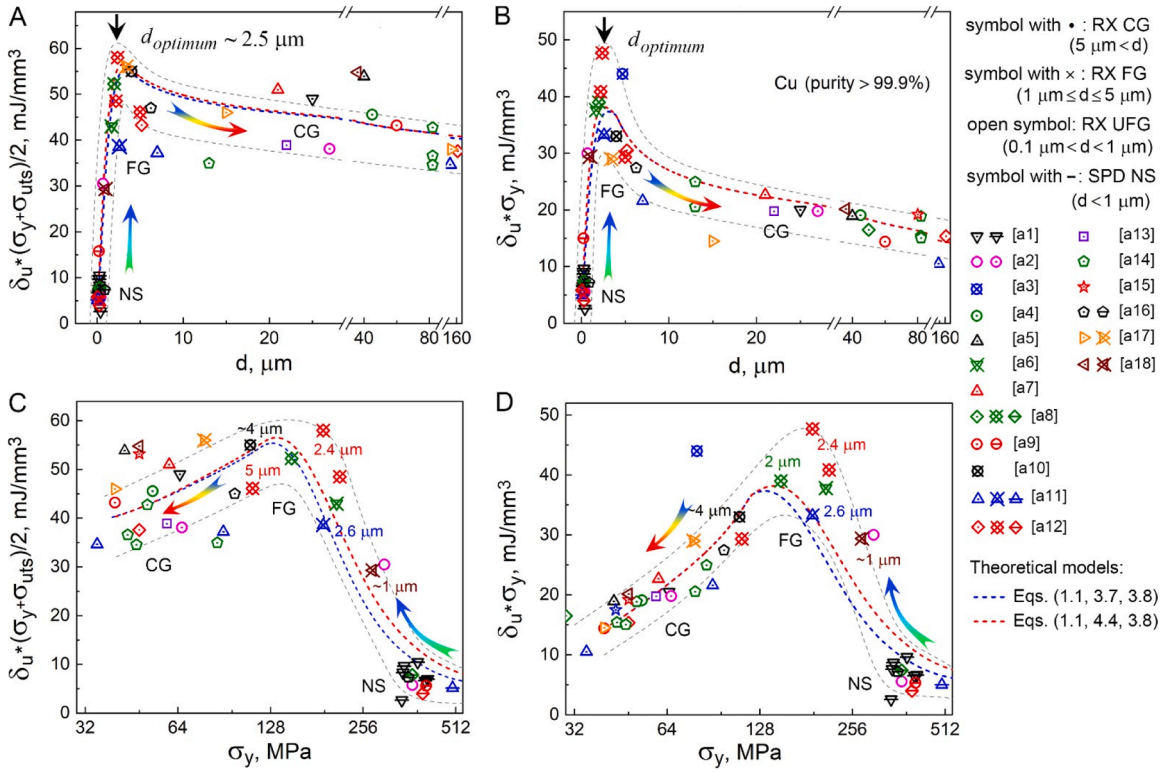

Fig. 2. *d*-dependent variation of (A) $\delta_u*\sigma_y$ and (B) $\delta_u*(\sigma_y+\sigma_{uts})/2$, showing the existence of $d_{optimum}$ in the FG regime for strength-ductility combination. (C) $\delta_u*\sigma_y$ and (D) $\delta_u*(\sigma_y+\sigma_{uts})/2$ plotted as a function of σ_y, showing that the superior strength-ductility combination at $d_{optimum}$ is achieved with high yield strength. The literatures numbered a1-a18 are same to those in Fig. 1. (For interpretation of the references to color in this figure legend, the reader is referred to the web version of this article.)

(both in grade I and grade II, Fig. S1), austenitic stainless steel (316 L, Fig. S2), pure Al with high stacking fault energy (SFE) (Fig. S3) and Cu-Al alloys with low SFE (Figs. S4 and S5). Strikingly, it is found that all materials share the similar grain size dependence of strength-ductility combination to that of pure Cu, i.e., displaying $\delta_u * (\sigma_y + \sigma_{uts})/2$ and $\delta_u * \sigma_y$ peaks soon after recrystallization from NS. Taking the bcc IF steel as an example, the $d_{optimum}$ appears at ~2.2 μm, away from which the properties are obviously dropped (Figs. 3*A-B*). The optimal strength-ductility combination is achieved at a high strength level several times that of CG materials, and it disappears rapidly if the yield strength increases beyond ~400 MPa (Figs. 3*C-D*). The $d_{optimum}$ and the properties at it are summarized in Table. 1. These observations suggest that the $d_{optimum}$ may exist ubiquitously in materials with different crystal structures.

It is noticed that the $d_{optimum}$ of most materials are in the FG regime, i.e., within 1–5 μm (Table. 1). Fig. 4*A*, in which only the data of RX UFG and RX FG are included, compares the $\delta_u * (\sigma_y + \sigma_{uts})/2$ peak among pure Cu, Cu-5Al and Cu-11Al. As shown, the $d_{optimum}$ decreases gradually with increasing Al content. In Fig. 4*B*, the $d_{optimum}$ of a series of fcc materials are plotted as a function of SFE, showing that lower SFE tends to confer smaller $d_{optimum}$.

The appearance of denser annealing twins may be responsible for the reduced $d_{optimum}$ when decreasing SFE. In fcc crystals, low SFE facilitates the formation of annealing twins during recrystallization (Mahajan, 1997; Tian et al., 2016), which act as obstacle and pathway for dislocation glide and thus produce strengthening and hardening effects simultaneously (Lu et al., 2009; Zhu et al., 2012). In other words, twin boundaries contribute to both higher strength and ductility while rendering the grain (crystal) size smaller, thereby enabling the best combination of strength and ductility at finer grain size. It should be noted that the increase of solute content in alloys may also be a potential factor for the change of the $d_{optimum}$ with SFE, since there are additional strengthening and hardening effects conferred by solid solution. These results and physics make it reasonable to believe that the $d_{optimum}$ of materials with high/-medium SFE should generally be within the FG regime, while lowering SFE gradually reduces it even to the UFG regime in extreme cases.

4. Theoretical model for predicting the $d_{optimum}$

The existence of $d_{optimum}$ has significant implications for the design and choice of structural materials for superior mechanical properties at minimum material cost. For example, a 316 L stainless steel structure can reduce its weight by a third, while carrying the same load without sacrificing the strain energy density limit, if its grain size is refined from ~40 μm to the critical size $d_{optimum}$ (~1.2

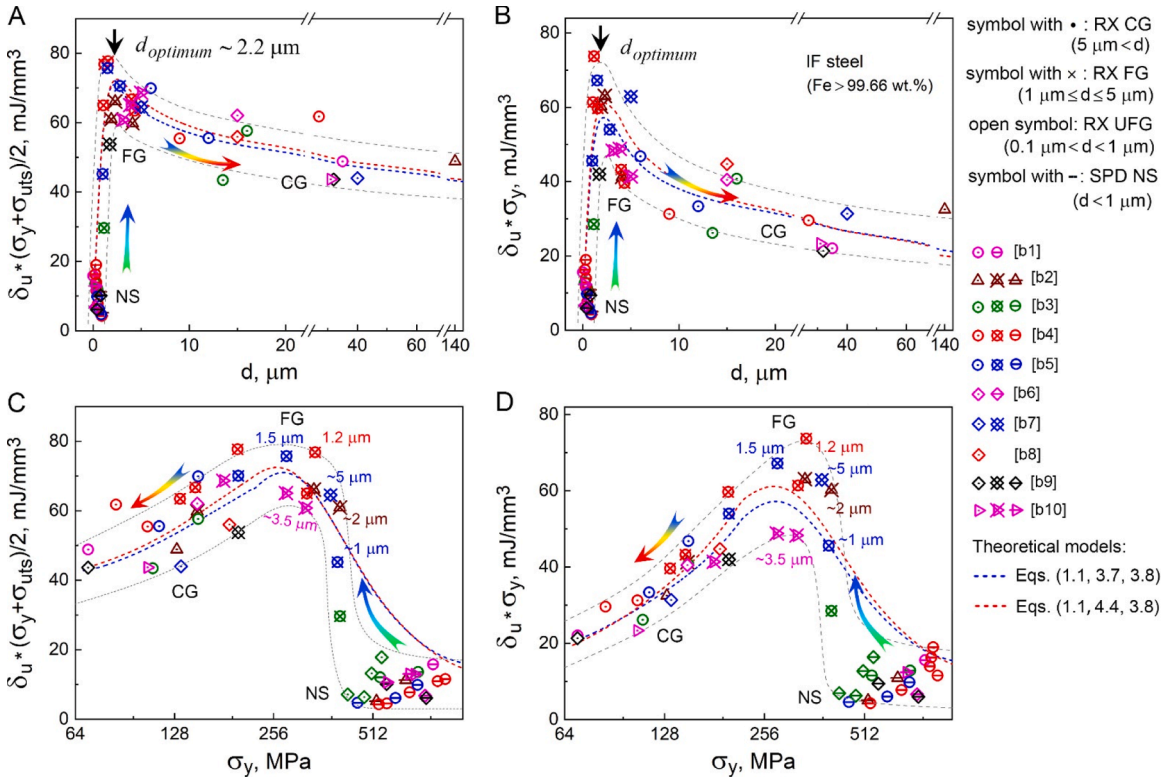

Fig. 3. The $d_{optimal}$ (~2.2 μm) of IF steel with a Fe content of >99.66 wt.%. d-dependent variation of (A) $\delta_u * \sigma_y$ and (B) $\delta_u * (\sigma_y + \sigma_{uts})/2$. (C) $\delta_u * \sigma_y$ and (D) $\delta_u * (\sigma_y + \sigma_{uts})/2$ versus σ_y. Experimental data are collected from the following literatures: b1 (Wu et al., 2014), b2 (Hazra et al., 2011), b3 (Yoda et al., 2011), b4 (Tsuji et al., 2002), b5 (Gao et al., 2014), b6 (Jiang et al., 2019), b7 (Sekban et al., 2015), b8 (Saray et al., 2011), b9 (Lee et al., 2004), b10 (Purcek et al., 2012). (For interpretation of the references to color in this figure legend, the reader is referred to the web version of this article.)

Table. 1
The $d_{optimum}$ and the corresponding best strength-ductility combination of materials with varying crystal structures and properties. The $\delta_u*(\sigma_y+\sigma_{uts})/2$ and $\delta_u*\sigma_y$ of hcp pure Ti, pure Al, 316 L stainless steel and Cu-Al alloys plotted against d and σ_y are collected in the Supplementary Materials.

Materials	Crystal type	SFE, (mJ/m^2)	$d_{optimum}$ (μm)	σ_y at $d_{optimum}$ (MPa)	$\delta_u*(\sigma_y+\sigma_{uts})/2$ at $d_{optimum}$ (mJ/mm^3)	$\delta_u*\sigma_y$ at $d_{optimum}$ (mJ/mm^3)
Pure Cu (>99.9 wt.%)	fcc	78.5	~2.5	~180	53±7	43±6
IF steel (>99.66 wt.%)	bcc	200	~2.2	~300	66±11	60±12
Pure Ti grade I or TA1	hcp	–	~3.2	72±9	~475	65±9
grade II or TA2		–	~3	104±12	~545	96±8
Pure Al (>99.4%)	fcc	166	~2	50–130	20±8	17±5
316 L stainless steel	fcc	27	~1.2	~600	265±55	230±45
Cu-5Al (4.5–5.0 at.% Al)	fcc	32–28	~1	~225	84±8	70±8
Cu-11Al (10.8–11.6 at.% Al)	fcc	10–8	~1	~300	130±23	106±14

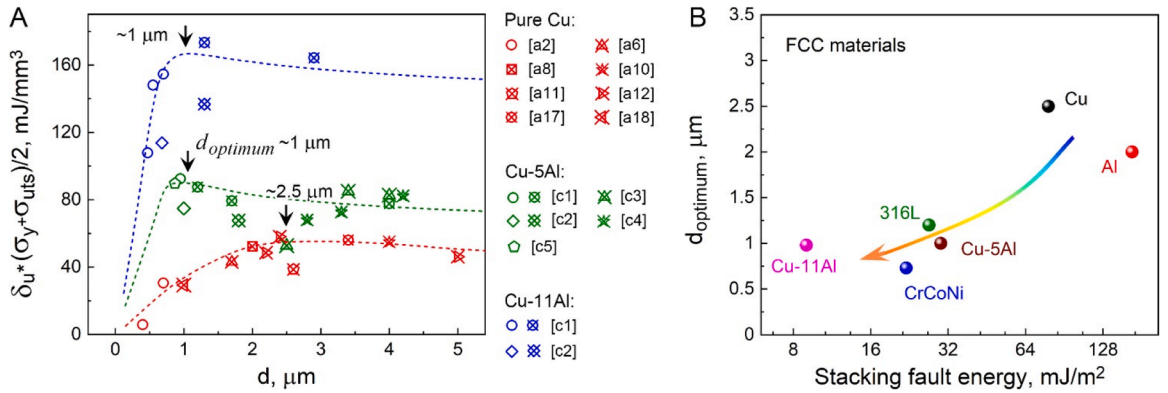

Fig. 4. Effect of SFE on the $d_{optimum}$. (A) Comparison of the d-dependent $\delta_u*(\sigma_y+\sigma_{uts})/2$ among pure Cu, Cu-5Al and Cu-11Al. (B) The variation of $d_{optimum}$ with decreasing SFE in FCC materials. The $d_{optimum}$ of CrCoNi was reported to be ~0.7 μm if twin boundary is included in grain size statistics (Guo et al., 2022). The literatures for the data of pure Cu are same to those in Fig. 1. Literatures for the data of Cu-Al alloys are: c1 (Tian et al., 2016), c2 (Liu et al., 2018), c3 (Ren et al., 2021), c4 (An et al., 2011), c5 (Lin et al., 2020). (For interpretation of the references to color in this figure legend, the reader is referred to the web version of this article.)

μm) (Fig. S2). To rationalize the existence of $d_{optimum}$ and predict it theoretically, a physics-based model is highly desired. The key to it should be the theoretical models representing the grain size dependence of σ_y, δ_u and σ_{uts}.

4.1. Grain size dependent σ_y

For the polycrystalline materials with dislocation-mediated yielding process, the dependence of σ_y on grain size can be represented by the Hall-Patch relationship

$$\sigma_y = \sigma_f + k_{HP}d^{-0.5}, \tag{1.1}$$

where σ_f is the lattice friction stress and k_{HP} is a fitted material constant, although the underlying physics are still under discussion (Dunstan and Bushby, 2014; Hansen, 2004; Meyers and Chawla, 2009). It has been proved that the Hall-Patch relationship is generally valid over a wide grain size range even down to tens of nanometers (Chen et al., 2006; Sanders et al., 1997). For pure Cu over the grain size range of $d > 0.1$ μm it can be well fitted by $\sigma_y = 25 + 190d^{-0.5}$ (the red dotted lines in Fig. 1*B*).

The effect of grain size on global flow stress (σ_{flow}) lies in the d-dependent σ_y and work hardening, as expressed by the Taylor relation

$$\sigma_{flow} = \sigma_f + k_{HP}d^{-0.5} + \beta\sqrt{\rho}, \tag{1.2}$$

where dislocation density ρ is a function of grain size and deformation history. $\beta = M\alpha Gb$, where M, α, G and b are Taylor factor, Taylor constant, shear modulus and the magnitude of Burgers vector, respectively.

4.2. Grain boundary affected region (Gbar)

The Considère criterion and the flow stress expression (Eq. (1.2)) suggest that the δ_u and σ_{uts} are governed by work hardening, whereas work hardening is determined by dislocation accumulation. Therefore, more attuned to the physical model of d-dependent δ_u

and σ_{uts} would be to track the grain boundary effects on dislocation accumulation.

Grain boundaries may act as both slip barriers and sources for dislocations (Cottrell, 1958; Murr, 2016). Meyer et al. (Fu et al., 2001; Meyersm and Ashworth, 1982) proposed that the inter-grain deformation incompatibility is capable of introducing high shear internal stress at grain boundaries, which helps to activate more dislocation slips in its vincity (Zhou et al., 2019). These effects collectively lead to the formation of a grain boundary affected region (Gbar) with unique dislocation accumulation and work hardening behaviors that are distinct from those in grain interior (Delincé et al., 2007; Fu et al., 2001; Hirth, 1972; Meyersm and Ashworth, 1982). As such, in the analysis of grain plasticity, a grain can be modeled as a composite of Gbar and grain interior if the diameter is larger than twice of the charactertstic width of Gbar (l_{Gbar}), i.e., $d > 2l_{Gbar}$, whereas the entire grain is composed of Gbar if $d \leq 2l_{Gbar}$ (Fig. 5).

The ratio l_{Gbar}/d determines the volume fraction of Gbar and thus is a key parameter controlling the intensity of grain boundary effects. Note that grain boundary-supported dislocation accumulation generally appears in a pile-up configuration (Hirth and Lothe, 1982a; Murr, 2016; Zhou et al., 2019), particularly at the low-strain stage. Grain boundary/dislocation interaction in Gbar is manifested as the pileups repelling incoming dislocations, while dislocations away from the pileup end is not affected much due to the quick attenuation of pile-up induced long-range back stress (Hirth and Lothe, 1982a; Mitchell, 1964; Zhu and Wu, 2019). Therefore, the l_{Gbar} can be logically considered equal to the saturation length of pile-up (l_{pileup}).

Upon loading, piling-ups against grain boundary occur before macro yielding (Fu et al., 2001; Meyersm and Ashworth, 1982). The length of a pile-up increases with increasing resolved external stress (τ_r) until the stress concentration at head reaches the strength of grain boundary (τ^*), beyond which the heading dislocation may transmit through it, or dislocation sources in adjacent grain may be activated, which relieves local stress concentration and thus removes the opportunity of further increasing pile-up length by increasing τ_r (Meyers and Chawla, 2009). Since the length of screw dislocation pile-up is often limited by cross-slipping (Adelman and Dundurs, 1973), here we consider the pile-up of perfect edge dislocations to obtain the upper limit of l_{pileup}, which should be more physically appropriate in representing the l_{Gbar}. Thus, the governing equation for l_{pileup} is

$$\frac{\pi(1-\nu)l_{pileup}\tau_r^2}{Gb} = \tau^* \tag{2.1}$$

in a single-ended pile-up of edge dislocations, where ν is the Poisson's ratio. The left term represents the stress concentration at pile-up head, equaling the product of the number of dislocations in the pile-up and the τ_r (Eshelby et al., 1951; Hirth and Lothe, 1982a).

Considering that for the small grains with d at or near submicron, the pile-up length is generally limited by the grain size, which can be statistically taken as half of the grain size, i.e., $l_{pileup} = d/2$. Since the whole grain is occupied by Gbar (piling-up region), the τ_r in such small grain can be considered to be uniform. Thus, if it is further assumed that macro yielding occurs when the stress concentration at the head of early pile-ups is high enough to yield the grain boundary (Meyers and Chawla, 2009), i.e., yielding when the length of early pile-ups reaches l_{pileup}, the τ_r at this critical state can be represented by the macroscopic yield strength as $\tau_r = \frac{k_{HP}d^{-0.5}}{M}$. Taking these two scenarios into account in Eq. (2.1) yields

$$\tau^* = \frac{\pi(1-\nu)\left(\frac{k_{HP}}{M}\right)^2}{2Gb}. \tag{2.2}$$

Although the τ^* is derived by analyzing a special case (small grains at yielding), it actually is a material constant valid for other grain size ranges and deformation states as well. Multiplying Taylor factor M yields the grain boundary strength σ^* in terms of normal stress, which can be considered as the strength limit of a polycrystalline aggregate in the size range with dislocation-dominated plasticity. The σ^* for Cu is estimated to be ~1 GPa, which is consistent with our common knowledge on the maximum strength of Cu.

While for large grains with $d > 2l_{Gbar}$, the τ_r in Gbar and grain interior should be different and thus cannot be evaluated based on the overall applied stress (Fu et al., 2001). For instance, the pile-up exerts extra back stress in Gbar, which requires higher τ_r to drive local deformation. We assume that pile-ups are mainly generated by Frank-Read sources. Thus, the τ_r at pile-up source equals the sum of the intrinsic bowing stress (τ_{F-R}) and the back stress exerted by piling-up dislocations (τ_b)

$$\tau_r = \tau_{F-R} + \tau_b, \tag{2.3}$$

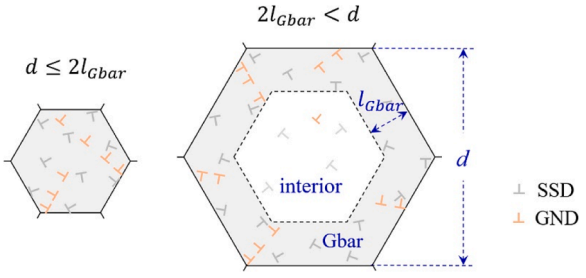

Fig. 5. A schematic illustrating the Gbar and grain interior. SSD and GND represent statistically stored dislocation and geometrically necessary dislocation, respectively. (For interpretation of the references to color in this figure legend, the reader is referred to the web version of this article.)

where $\tau_{F-R} = Gb/R$, and R is the distance between the pinning points of source (Hull and Bacon, 2011). The source is assumed to be outside the pileup, with a limited distance on the order of R from pileup end. The τ_b thus can be obtained by a standard integration of the interaction stress of piling-up dislocations. The result is (Hirth and Lothe, 1982a)

$$\tau_b = \tau_r \left(1 - \sqrt{\frac{R}{R + l_{pileup}}}\right). \tag{2.4}$$

Combining Eqs. (2.3) and (2.4) yields

$$\tau_r = \tau_{F-R} \sqrt{\frac{R + l_{pileup}}{R}}. \tag{2.5}$$

Substituting Eqs. (2.2) and (2.5) into (2.1) gets

$$l_{pileup} = \frac{1}{2}\left(\frac{k_{HP}}{M\tau_{F-R}}\right)^2 \frac{R}{R + l_{pileup}}. \tag{2.6}$$

The l_{pileup} observed in CG under electron microscope is generally on the order of microns (Murr and Wang, 1982; Otto et al., 2013), whereas R is usually on the order of submicrons as approximated by the average spacing of dislocations (Hirth and Lothe, 1982b; Hull and Bacon, 2011). Thus, $\frac{R}{R+l_{pileup}}$ can be approximated by $\frac{R}{l_{pileup}}$. Plugging the bowing stress into it leads to

$$l_{pileup} \approx \frac{k_{HP} R^{3/2}}{\sqrt{2} MGb}. \tag{2.7}$$

Therefore, we have

$$l_{Gbar} \approx \frac{k_{HP} R^{3/2}}{\sqrt{2} MGb}. \tag{2.8}$$

l_{Gbar} is estimated to be on the order of a few micrometers. For instance, taking R to be about $10^3 b$ such as ~0.5 μm and $k_{HP} = 190$ MPa · $\mu m^{0.5}$ for CG Cu, l_{Gbar} is ~1.4 μm. Taking $k_{HP} = 500$ MPa · $\mu m^{0.5}$ for 304 stainless steel, l_{Gbar} is calculated to be ~2.1 μm, which is almost exactly the experimentally measured average length of grain boundary-supported pileups by Murr et al. (Murr, 2016; Murr and Wang, 1982). Note that the deviation in l_{Gbar} introduced by the approximation of $\frac{R}{R+l_{pileup}}$ by $\frac{R}{l_{pileup}}$ is typically less than ~10%, and it does not exceed 11% even for a material like 304 stainless steel for which the $\frac{k_{HP}}{\tau_{F-R}}$, a key factor controlling the deviation, is extremely high.

Eq. (2.8) suggests that l_{Gbar} is a material constant determined primarily by grain boundary strength and dislocation source property. Murr et al. has found that the average length of grain boundary-supported pileups remains largely constant in the plastic stage (Murr, 2016; Murr and Wang, 1982). These observations convince us that l_{Gbar} is independent of plastic deformation history. It should be noted that, at macro yielding, the attainment of τ^* by early pileup indicates the local grain boundary, rather than the whole, cannot withstand more dislocations joining the pileup. In other words, there is an opportunity to form more pileups in Gbar in the plastic stage (Murr, 2016; Wang et al., 2020).

4.3. Grain size dependent δ_u and σ_{uts}

Here dislocation evolution laws for Gbar and grain interior are developed based on the Kocks-Mecking-Estrin model and the extension made by Li et al. (Estrin et al., 1998; Estrin and Mecking, 1984; Kocks, 1976; Li et al., 2017; Li and Soh, 2012; Mecking and Kocks, 1981). Specifically, the original mean-filed model is simplified for different grain size intervals by distinguishing the major dislocation multiplication and recovery terms in the two regions based on the underlying physics.

In the size range of $d \leq 2l_{Gbar}$, grain is entirely composed of Gbar, and dislocation activities are grain boundary-affected processes, as analyzed above. Filtering out the terms independent of grain boundary effects from the extended Kocks-Mecking-Estrin model yields the governing equation of dislocation density (ρ_{Gbar}) evolution for such small grains,

$$\frac{\partial \rho_{Gbar}}{\partial \varepsilon_{Gbar,p}} = M\left[\frac{k_0}{bd} - k_1\left(\frac{l_{Gbar}}{d}\right)^2 \rho_{Gbar}\right], \tag{3.1}$$

where $\varepsilon_{Gbar,p}$ is the plastic strain, while k_0 and k_1 are material constants. The first term on the right side describes dislocation storage rate, which is proportional to grain boundary density; this term has been validated by the observations that the mean free slip path of dislocations in small grains is largely determined by grain size (Estrin and Mecking, 1984; Mecking and Kocks, 1981). The last term accounts for the grain boundary-assisted recovery (Li and Soh, 2012; Zhao et al., 2020), which has been widely used to represent the quick dislocation saturation and corresponding plasticity of UFG/NS materials (Li et al., 2020; Malygin, 2007; Valiev et al., 1994). Integrating Eq. (3.1) obtains the expression for ρ_{Gbar}. Substituting it into Eq. (1.2) and then implementing the initial condition, $\sigma_{Gbar} = \sigma_y$ at $\varepsilon_{Gbar,p} = 0$, gives the expression of flow stress σ_{Gbar}

$$\sigma_{Gbar} = \sigma_y + \beta\sqrt{\frac{k_2}{k_3}\left[1 - \exp\left(-k_3\varepsilon_{Gbar,p}\right)\right]}. \tag{3.2}$$

where $k_2 = \frac{Mk_0}{bd}$, and $k_3 = Mk_1\left(\frac{l_{Gbar}}{d}\right)^2$. The limit of uniform plastic strain $\varepsilon_{Gbar,pu}$, therefore, can be derived based on the Considère criterion $\frac{\partial\sigma_{Gbar}}{\partial\varepsilon_{Gbar,p}} = \sigma_{Gbar}$ as

$$\varepsilon_{Gbar,pu} = -\frac{1}{k_3}\ln\left\{1 - \frac{k_3}{\beta^2 k_2}\left[\frac{\sqrt{\sigma_y^2 + \beta^2 k_2(2+k_3)} - \sigma_y}{2+k_3}\right]^2\right\}. \tag{3.3–1}$$

Then, substituting $\varepsilon_{Gbar,pu}$ into Eq. (3.2) obtains the strength at the end of uniform deformation

$$\sigma_{Gbar,pu} = \sigma_y + \frac{\sqrt{\sigma_y^2 + \beta^2 k_2(2+k_3)} - \sigma_y}{2+k_3}. \tag{3.3–2}$$

Obviously, the $\varepsilon_{Gbar,pu}$ and $\sigma_{Gbar,pu}$ can be explicitly represented as functions of d. Note that, for a pre-strained material with initial dislocation density of ρ_0 the $\varepsilon_{Gbar,pu}$ and $\sigma_{Gbar,pu}$ can also be derived by changing the initial condition as $\sigma_{Gbar} = \sigma_y + M\alpha\mu b\sqrt{\rho_0}$ at $\varepsilon_{Gbar,p} = 0$. The results will show that pre-strain only affect the residual $\varepsilon_{Gbar,pu}$ while $\sigma_{Gbar,pu}$ remains unchanged.

In the Gbar of grains in the size range of $d > 2l_{Gbar}$, dislocation evolution and stress-strain response should be same to those of a grain at the critical size of $d = 2l_{Gbar}$, since in both cases the grain boundary effect manifests itself to the greatest extent. In other words, the plastic behavior of Gbar in such large grains can also be described by Eqs. (3.1-3.3) adopting a virtual parameter $d = 2l_{Gbar}$. Thus, the uniform plastic strain limit and corresponding strength limit of Gbar in large grains are, respectively, numerically equal to the $\varepsilon_{Gbar,pu}$ and $\sigma_{Gbar,pu}$ at $d = 2l_{Gbar}$, hereafter being referred to as $\varepsilon^c_{Gbar,pu}$ and $\sigma^c_{Gbar,pu}$.

In grain interior, dislocation evolution depends primarily on local dislocation density and not affected by grain boundary, so it can be represented by the classical Kocks-Mecking model (Kocks, 1976; Mecking and Kocks, 1981)

$$\frac{\partial\rho_{int}}{\partial\varepsilon_{int,p}} = M\left(\frac{k_4}{b}\sqrt{\rho_{int}} - k_5\left(\dot{\varepsilon}_{int,p}, T\right)\rho_{int}\right). \tag{3.4}$$

The storage rate (the first term on the right side) is considered inversely proportional to the mean slip path $\rho_{int}^{-1/2}$ with a factor of k_4. The last term describes the recovery rate in which the factor k_5 is a function of temperature and strain rate. By integrating Eq. (3.4) and then implanting the resulting ρ_{int} into the local flow stress expression $\sigma_{int} = \sigma_f + \beta\sqrt{\rho_{int}}$ with an initial condition that $\sigma_{int} = \sigma_f$ at $\varepsilon_{int,p} = 0$, one readily obtains the flow stress of grain interior

$$\sigma_{int} = \sigma_f + \frac{\beta k_6}{k_7}\left[1 - \exp\left(-\frac{k_7\varepsilon_{int,p}}{2}\right)\right], \tag{3.5}$$

where $k_6 = M\frac{k_4}{b}$ and $k_7 = Mk_5(\dot{\varepsilon}_{int,p}, T)$. This is actually a natural exponential expression of stress-strain relationship in the form of $\sigma = \sigma_0 + ke^{n\varepsilon}$. Then, the limit of uniform plastic strain $\varepsilon_{int,pu}$ and the corresponding strength limit $\sigma_{int,pu}$ are, respectively, derived as

$$\varepsilon_{int,pu} = -\frac{2}{k_7}\ln\left[\frac{\frac{\beta k_6}{k_7} + \sigma_f}{\left(1 + \frac{k_7}{2}\right)\frac{\beta k_6}{k_7}}\right] \tag{3.6.1}$$

and

$$\sigma_{int,pu} = \frac{\beta k_6 + k_7\sigma_f}{2 + k_7}. \tag{3.6.2}$$

Clearly, these two properties are also d-independent constants.

The different dislocation accumulation behaviors in the Gbar and grain interior render inhomogeneous intragranular plasticity. For example, the Gbar may be work hardened in a higher rate and reach flow stress saturation at an earlier stage of global strain than those of grain interior (Fu et al., 2001; Meyersm and Ashworth, 1982). Here we assume that the onset of global instability can only occur when both the Gbar and the grain interior reach flow stress saturation. Accordingly, the global limit of uniform plastic strain ε_{pu} can be approximated as the area fraction-weighted average of the saturation strains of Gbar and grain interior, i.e.

$$\varepsilon_{pu} = \begin{cases} \varepsilon_{Gbar,pu} & (d \le 2l_{Gbar}) \\ S_{Gbar}\varepsilon^c_{Gbar,pu} + (1 - S_{Gbar})\varepsilon_{int,pu} & (d > 2l_{Gbar}) \end{cases}, \tag{3.7.1}$$

where $S_{Gbar} = 1 - (d - 2l_{Gbar})^3/d^3$ is the average area fraction of Gbar on the across-section of a polycrystalline sample. Similarly, the global strength limit σ_{pu} at ε_{pu} is

$$\sigma_{pu} = \begin{cases} \sigma_{Gbar,pu} & (d \le 2l_{Gbar}) \\ S_{Gbar}\sigma^{c}_{Gbar,pu} + (1 - S_{Gbar})\sigma_{int,pu} & (d > 2l_{Gbar}) \end{cases}. \tag{3.7.2}$$

The above analysis is conducted in terms of true stress and true plastic strain. By adding the elastic part and then transforming into engineering response, one obtains the δ_u

$$\delta_u = \exp\left(\varepsilon_{pu} + \frac{\sigma_y}{E}\right) - 1, \tag{3.8.1}$$

and the σ_{uts}

$$\sigma_{uts} = \sigma_{pu}/(1 + \delta_u). \tag{3.8.2}$$

The models here provide explicit expressions of δ_u and σ_{uts} with d as the only variable. The grain size dependence and the underlying mechanism are clearly indicated. For small grains with $d \le 2l_{Gbar}$, the dependence originates from the grain boundary effects on dislocation accumulation, whereas it is primarily due to the change of the area ratio of Gbar and grain interior when $d > 2l_{Gbar}$.

The blue curves in Figs. 1*A* and *C* are determined by Eqs. (3.7–3.8) using the parameters listed in Table. 2, which give reasonable fits to the experimental data of δ_u and σ_{uts}. The blue curves in Figs. 2 and 3 represent the predicted $\delta_u * (\sigma_y + \sigma_{uts})/2$ and $\delta_u * \sigma_y$ by combining Eqs. (1.1), (3.7) and (3.8), which, both numerically and in the variation, are in good agreement with experimental results. The predicted $d_{optimum}$ for pure Cu and IF steel are ~3.0 μm and ~2.4 μm, respectively. These comparisons confirm that the theoretical models are valid and successful in representing the grain size dependence of δ_u and σ_{uts}, predicting the $d_{optimum}$, and predicting the strength-ductility combination. Interestingly, the predicted $d_{optimum}$ are very close to $2l_{Gbar}$, i.e., $d_{optimum} \approx 2l_{Gbar}$.

4.4. Semi-empirical expressions for grain size dependent $\boldsymbol{\delta_u}$ and $\boldsymbol{\sigma_{uts}}$

To obtain compact yet still physically meaningful models on the grain size dependence of δ_u and σ_{uts} so as to be more attuned to engineering application, further efforts are made to simplify the expressions in Eqs. (3.7). In the expression of $\varepsilon_{Gbar,pu}$ (Eq. (3.3–1)), σ_y ($\sim 10^2 d^{-1/2}$ MPa) is a small term as compared to $\beta\sqrt{k_2(2 + k_3)}$ (generally $> 10^3 d^{-1/2}$ MPa). Ignoring this small term yields a concise expression as

$$\varepsilon_{Gbar,pu} \approx -\frac{d^2}{Ml^2_{Gbar}} \ln\left(\frac{d^2}{d^2 + Ml^2_{Gbar}/2}\right). \tag{4.1}$$

Table. 2
Material parameters required for the theoretical models (Eqs. (3.7) & (3.8)), in pure Cu and IF steel.

Parameter	Pure Cu	IF steel	Access
Shear modulus, G (MPa)	$42.1*10^3$	$76.9*10^3$	Physical parameters
Burgers vector, b (μm)	$0.256*10^{-3}$	$0.26*10^{-3}$	
Taylor constant, α	0.3	0.3	
Taylor factor, M	3.06	3.06	
Lattice friction stress, σ_f (MPa)	25	45	
Characteristic width of Gbar, l_{Gbar} (μm)	1.4	1.3	
Hall-Patch slope, k_{HP} (Mpa $\cdot$ $\mu m^{0.5}$)	190	330	Empirical/fitting constants
Geometric factor, k_0	0.38	0.54	
Grain boundary-assisted recovery factor, k_1	1	0.7	
Proportionality factor, k_4	0.026	0.043	
Dynamic recovery factor, k_5	3.8	5.8	

Note that the partition of Gbar and grain interior make the models explicit and concise. An attendant embarrassment here is that the reciprocal of the piecewise representations (Eqs. (3.7)) is discontinuous at $d = 2l_{Gbar}$, but fortunately it appears to have little influence on the predictions of the overall dependence of δ_u, σ_{uts} and their combination on d (Figs. 1–3). Eqs. (3.1) and (3.2) describe the dislocation evolution and flow stress response of Gbar in a mean-filed manner. Such treatment maintains the model concise but ignores the effects of dislocation inhomogeneity. As discussed later, dislocation inhomogeneity in Gbar is also partially responsible for the optimal strength-ductility combination at the $d_{optimum}$. There is another possible limitation for the above derivation. For the deformation of UFG and NS, we only considered the dislocation mechanism, while the possible effects conferred by grain boundary activities such as sliding, rotation and migration were largely ignored. But it is also believed that this omission may has little effect on predicting the grain size dependence of δ_u and σ_{uts}, since the extended Kocks–Mecking–Estrin model, which incorporated the grain size effects, has been proved to be effective in describing the property of grains as small as a few hundred nanometers (Li et al., 2017; Li and Soh, 2012; Zhao et al., 2020).

Reconsidering that σ_y in Eq. (3.3–1) increases the natural number of the logarithmic function, Eq. (4.1) will provide an exaggerated $\varepsilon_{Gbar,pu}$. Therefore, it is further modified by implanting a correction coefficient A to recall the effect of σ_y

$$\varepsilon_{Gbar,pu} = -\frac{d^2}{Ml_{Gbar}^2}\ln\left(\frac{d^2}{d^2+A}\right), \tag{4.2}$$

where A should be smaller than $Ml_{Gbar}^2/2$. $\varepsilon_{BA,pu}^c$ is updated accordingly as

$$\varepsilon_{Gbar,pu}^c = -\frac{4}{M}\ln\left(\frac{4l_{Gbar}^2}{4l_{Gbar}^2+A}\right). \tag{4.3}$$

As detailed in the expression (Eq. (3.6–1)), $\varepsilon_{int,pu}$ is independent of grain size. It can thus be globally considered as a material constant determined by dislocation accumulation capability, being denoted as $\varepsilon_{int,pu}^0$. The physical meaning of $\varepsilon_{int,pu}^0$ suggests that its value approximates the uniform plastic elongation of a material with ultra-large grains.

Therefore, updating Eq. (3.7–1) yields a compact semi-empirical expression for ε_{pu}

$$\varepsilon_{pu} = \begin{cases} -\dfrac{d^2}{Ml_{Gbar}^2}ln\left(\dfrac{d^2}{d^2+A}\right) & (d \le 2l_{Gbar}) \\ S_{Gbar}\varepsilon_{Gbar,pu}^c + (1-S_{int})\varepsilon_{int,pu}^0 & (d > 2l_{Gbar}) \end{cases}, \tag{4.4.1}$$

which contains only one variable (d), one empirical parameter (A), and two pending physical constants (l_{Gbar} and $\varepsilon_{int,pu}^0$).

Similar analyses of the terms in Eq. (3.7–2) render a semi-empirical expression for σ_{pu}

$$\sigma_{pu} = \begin{cases} \sigma_y + \beta\sqrt{\dfrac{Cd}{2d^2+Ml_{Gbar}^2}} & (d \le 2l_{Gbar}) \\ S_{Gbar}\sigma_{Gbar,pu}^c + (1-S_{Gbar})\sigma_{int,pu}^0 & (d > 2l_{Gbar}) \end{cases} \tag{4.4.2}$$

C is also an empirical correction coefficient, which is on the order of $0.1M/b$ and physically related to the grain boundary-assisted dislocation multiplication in Gbar. The constant $\sigma_{int,pu}^0$ is a denotation of Eq. (3.6–2), i.e., the saturation flow stress of grain interior, which is numerically approximated by that of a material with ultra-large grains. $\sigma_{Gbar,pu}^c = \sigma_y + \beta\sqrt{\frac{2C}{(8+M)l_{Gbar}}}$, representing the saturation flow stress of Gbar in grains with $d > 2l_{Gbar}$.

The red curves in Figs. 1-3 are obtained by combining Eqs. (1.1), (3.8) and (4.4) using the parameters listed in Table. 3. As shown, the semi-empirical models provide reasonable predictions on the grain size dependent δ_u and σ_{uts} (Figs. 1*A* & *C*), the $d_{optimum}$ and the optimized strength-ductility combination in FG regime (Figs. 2-3) as well. As compared to Eqs. (3.7), the expressions and the empirical parameters in Eqs. (4.4) are largely reduced, whereas the newly introduced physical parameters, such as the $\varepsilon_{int,pu}^0$ and $\sigma_{int,pu}^0$, are more meaningful. These results and comparisons suggest that the semi-empirical models expressed by Eqs. (4.4) are valid and more attuned to engineering applications, in denoting the grain size dependence of δ_u and σ_{uts} and predicting the $d_{optimum}$.

5. Discussion

5.1. Microstructural physics for the best strength-ductility combination at $d_{optimum}$

The optimal strength-ductility combination at the $d_{optimum}$ can be attributed to the unique microstructure. First, the FG has considerably high grain boundary density, which results in high σ_y values several times that of CG (Figs. 1*B* & 2*C-D*). Second, the recrystallized FG has ample room for dislocation storage, and at the same time the high-density grain boundary can effectively block dislocations to ensure a high storage rate. These effects lead to high dislocation hardening to retain ductility. Fig. 6 shows the grain size

Table. 3
Independent parameters required for the semi-empirical models (Eqs. (4.4)), in pure Cu and IF steel.

Parameter	Pure Cu	IF steel	Access
Characteristic width of Gbar, l_{Gbar} (μm)	2	1.9	Physical parameters
Uniform plastic elongation of grain interior, $\varepsilon_{int,pu}^0$	0.31	0.24	
Saturation flow stress of grain interior, $\sigma_{int,pu}^0$ (MPa)	245	310	
Strain correction coefficient, A (μm^2)	3.4	2.8	Empirical/fitting constants
Stress correction coefficient, C (μm^{-1})	4400	3200	

dependence of strain hardening exponent, verifying that the strain hardening capability indeed recovers quickly to near saturation in the FG regime. Third, the $d_{optimum}$ may be exactly at the critical dimension enabling the most efficient development of intragranular plastic strain gradient, which are expected to generate strong back stress strengthening and hardening (Wang et al., 2018b; Zhao et al., 2020; Zhu and Wu, 2019), as analyzed in the next subsection.

5.2. Strong plastic strain gradient effect enabled by the $d_{optimum}$

The Gbar is characterized by GND pile-ups (Section 3.2). GND accumulation is accompanied by the developments of plastic strain gradient (Ashby, 1970; Ma et al., 2016; Wang et al., 2019c). The derivation of l_{Gbar} suggests that it actually is an inherent internal material length representing the grain boundary's capability to withstand the accumulation of plastic strain gradient and/or the GND piling-up, which is physically consistent with the material length l introduced in the strain gradient plasticity to scale the strain gradient effect (Gao et al., 1999; Huang et al., 2004; Hutchinson and Fleck, 1997; Nix and Gao, 1998). As discussed by Gao et al. (Gao et al., 1999), the contribution of strain gradient, symbolically represented as $ld\varepsilon/dx \sim \varepsilon(l/D)$, becomes dominant as the characteristic length of deformation field D is comparable to l. In micromechanical tests, D usually corresponds to the smallest geometric dimension of deformation field, such as the beam thickness in micro-bending and the wire radius in micro-twisting (Hutchinson and Fleck, 1997). While in the uniform tension of a polycrystalline aggregates, D could be taken as the half period of the inhomogeneous strain field at grain scale, i.e., $D \sim d/2$, where d is the grain size. Thus, strong strain gradient effect is theoretically expected when $d/2$ approaches l_{Gbar}, i.e., at $d \sim 2l_{Gbar}$, which is exactly in the FG regime and close to the $d_{optimum}$.

In the plastic stage, more and more pileups will form against grain boundary in the virginal locations until the flow stress of Gbar reaches saturation (Murr, 2016; Zhou et al., 2019), resulting in an enhancement of GND density gradient and plastic strain gradient (Fig. 7*A*) (Ma et al., 2016; Wang et al., 2020). Consequently, high back stress, scaled by $\tau_b \sim Gbl_{Gbar}^2 \frac{\partial \rho_{GND}}{\partial x}$ (Bayley et al., 2006; Y. F. Wang et al., 2022), is developed in Gbar (Fig. 7*B*).

Fig. 8 illustrates the grain size dependent distribution of plastic strain gradient, dislocations density gradient and back stress. In the CG regime with $d > 2l_{Gbar}$, the average plastic strain gradient and back stress are small due to the existence of broad grain interior. For the NS or UFG with $d \ll 2l_{Gbar}$, the overlapping of Gbars from opposite grain boundaries would mutually screen the piling-up of GNDs, which offsets the accumulation of dislocation density gradient, although high global dislocation density is rendered by the short slip path (Figs. 8*A* and *B*). Such screening effect consequently limits the development of back stress. While in the FG regime with $d \sim 2l_{Gbar}$, i.e., at the $d_{optimum}$ (Table. 1 and Eq. (2.8)), there is neither redundant grain interior nor severe overlap of Gbars, and the fully developed strain gradient zone approaches saturation (Figs. 8*A* and *B*). Thus, it is logically reasonable to expect the highest back stress effects (Fig. 8*C*). In other words, the $d_{optimum}$ may be associated with the critical grain size with the strongest strain gradient, and the best combination of strength and ductility at the $d_{optimum}$ originates largely from the strain gradient effects.

As mentioned earlier, the plots of $\delta_u * (\sigma_y + \sigma_{uts})/2$ and $\delta_u * \sigma_y$ versus grain size (Figs. 2, 3 & S1-S5) essentially reflect the grain size dependence of strain energy density limit, and the prominent peaks disclose that the critical grain size with the highest strain energy density limit is exactly the $d_{optimum}$ for strength-ductility combination. This advocates a new design concept following the mechanical principle: to optimize strength-ductility combination the microstructure should be engineered to maximize the strain energy density limit, such as tuning the grain size of constituent zone towards the possible $d_{optimum}$.

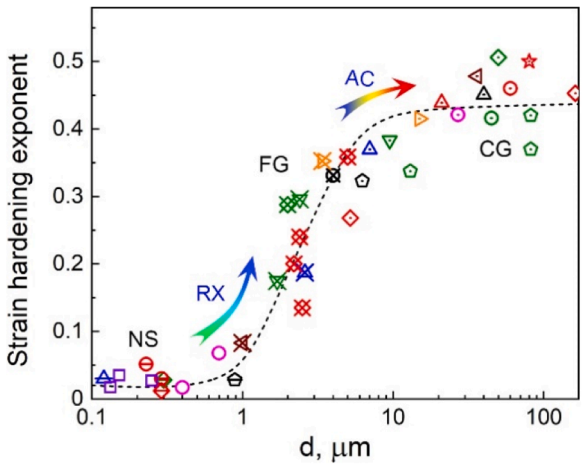

Fig. 6. The grain size dependence of strain hardening exponent of pure Cu, revealing the quick improvement of work hardening capability in the FG regime. The legend is same to that of Fig. 1. (For interpretation of the references to color in this figure legend, the reader is referred to the web version of this article.)

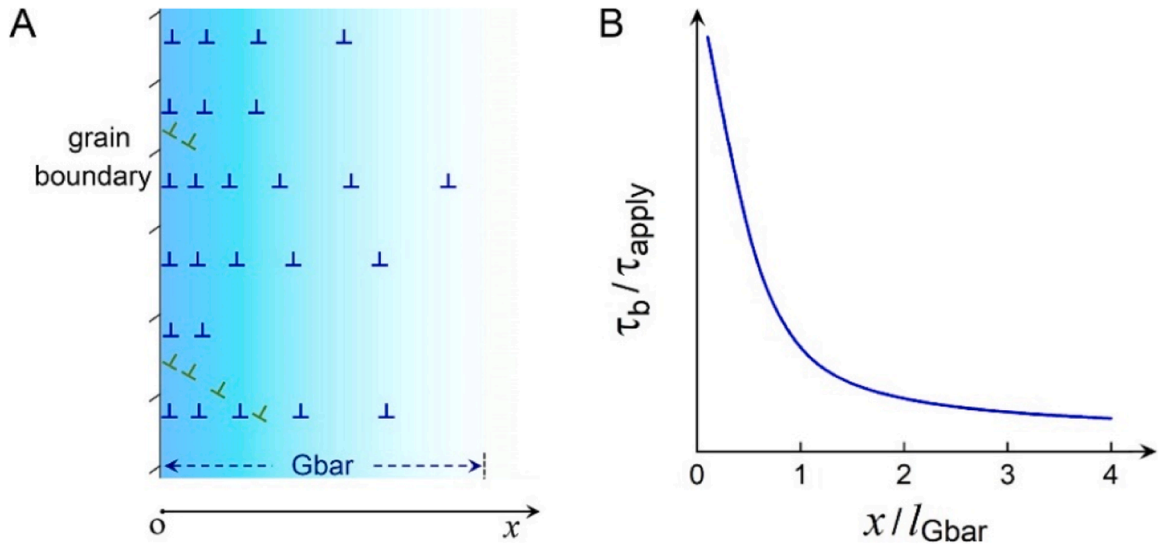

Fig. 7. Illustrations of (A) GND pile-ups in Gbar and (B) the resulting intragranular back stress. (For interpretation of the references to color in this figure legend, the reader is referred to the web version of this article.)

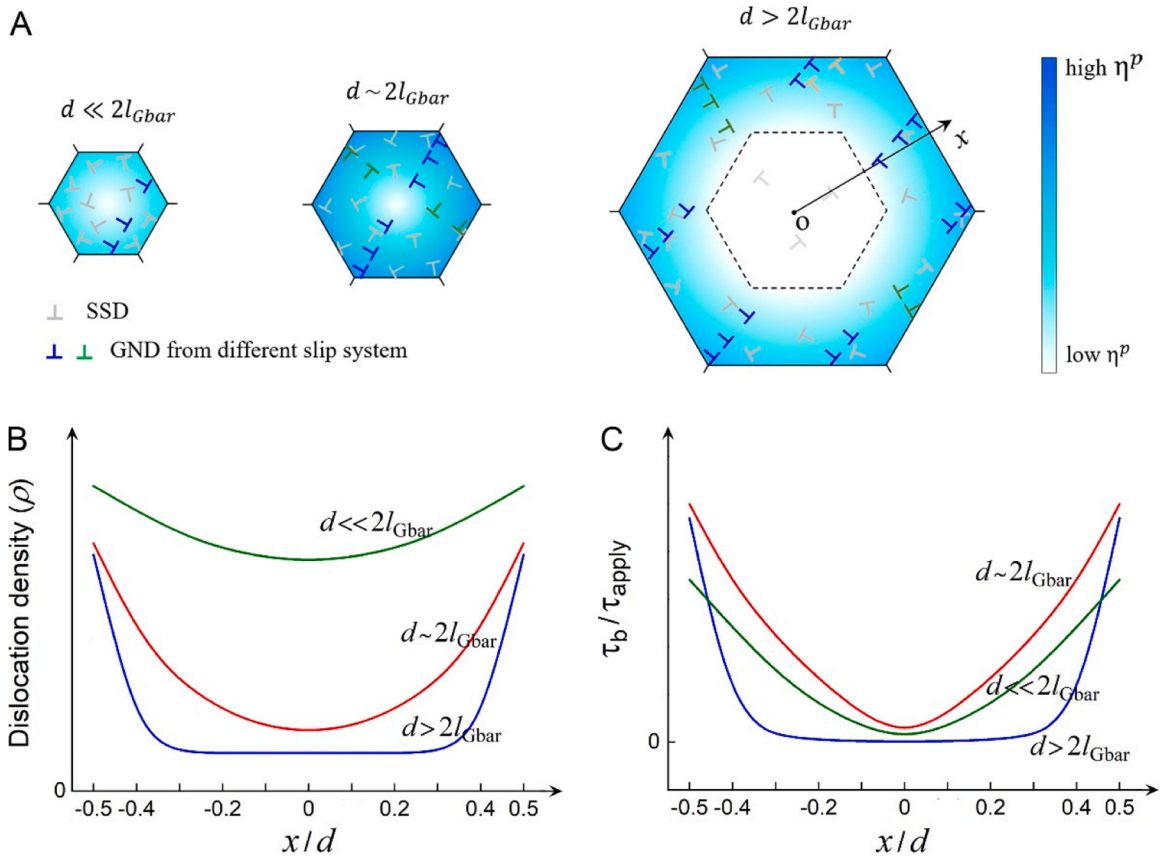

Fig. 8. Illustrations for the D-dependent distribution of (A) plastic strain gradient η^p, (B) dislocation density gradient and (C) back stress τ_b, at the same applied strain. (For interpretation of the references to color in this figure legend, the reader is referred to the web version of this article.)

6. Conclusion

In summary, the grain size dependence of tensile properties are systematically analyzed in a series of single-phase materials to investigate the optimum grain size ($d_{optimum}$) for strength-ductility combination, which can be indexed by the strain energy density limit such as by the products of strength and uniform elongation, $\delta_u * (\sigma_y + \sigma_{uts})/2$ and $\delta_u * \sigma_y$. Specifically, particular attention was devoted to verifying the existence, seeking the exact value, establishing the theoretical prediction models and probing the underlying deformation physics of the $d_{optimum}$. The main findings are:

(i) The $d_{optimum}$, generally on the order of a few micrometers, may exist ubiquitously in materials with different crystal structures. At the $d_{optimum}$, the strain energy density limit reaches a maximum while maintaining fairly high yield strength, achieving the optimal strength-ductility combination. The $d_{optimum}$ decreases slightly with decreasing stacking fault energy.

(ii) Theoretical models on the grain size-dependence of uniform elongation and ultimate strength are established by considering the difference of dislocation accumulation in grain boundary affected region (Gbar) and grain interior. Combined with the Hall-Petch relationship, the models provide accurate prediction on the $d_{optimum}$. The theoretical models are finally compacted into semi-empirical models each containing only one empirical material parameter, which are convenient for engineering application.

(iii) $d_{optimum} \approx 2l_{Gbar}$, where l_{Gbar} is the characteristic width of Gbar determined by the capability of grain boundary to withstand GNDs piling-up or strain gradient accumulation. This suggests that the $d_{optimum}$ is exactly at or near the critical grain size having the strongest intragranular plastic strain gradient effect. Moreover, the $d_{optimum}$ is also the limiting dimension that allows simultaneous strengthening and toughening by grain refinement, beyond which further strengthening will be at the severe expense of tension toughness.

CRediT authorship contribution statement

Yanfei Wang: Conceptualization, Methodology, Data curation, Writing – original draft, Writing – review & editing. **Chongxiang Huang:** Conceptualization, Formal analysis, Data curation. **Xiaolong Ma:** Conceptualization, Formal analysis, Data curation, Validation, Writing – original draft. **Jianfeng Zhao:** Methodology, Investigation. **Fengjiao Guo:** Methodology, Data curation. **Xiaotian Fang:** Formal analysis, Data curation, Writing – original draft. **Yuntian Zhu:** Conceptualization, Writing – review & editing, Funding acquisition. **Yueguang Wei:** Conceptualization, Writing – review & editing, Funding acquisition, Supervision.

Declaration of Competing Interest

The authors declare that they have no known competing financial interests or personal relationships that could have appeared to influence the work reported in this paper.

Data availability

Data will be made available on request.

Acknowledgements

This work was supported by the NSFC Programs (Nos. 12102006, 11890681, 12032001, 11521202, 51931003), the National Key R&D Program of China (2021YFA1200202), the Hong Kong Research Grants Council (GRF 11214121), and the Postdoctoral Science Foundation of China (Nos. 2020M680223, BX2021011).

Supplementary materials

Supplementary material associated with this article can be found, in the online version, at doi:10.1016/j.ijplas.2023.103574.

References

Adelman, N.T., Dundurs, J., 1973. Instability of screw dislocation pile-ups. J. Appl. Phys. 44, 5631–5632. https://doi.org/10.1063/1.1662213.

An, X.H., Qu, S., Wu, S.D., Zhang, Z.F., 2011. Effects of stacking fault energy on the thermal stability and mechanical properties of nanostructured Cu–Al alloys during thermal annealing. J. Mater. Res. 26, 407–415. https://doi.org/10.1557/jmr.2010.39.

An, X.H., Wu, S.D., Zhang, Z.F., Figueiredo, R.B., Gao, N., Langdon, T.G., 2012. Enhanced strength–ductility synergy in nanostructured Cu and Cu–Al alloys processed by high-pressure torsion and subsequent annealing. Scr. Mater. 66, 227–230. https://doi.org/10.1016/j.scriptamat.2011.10.043.

Ashby, M.F., 1970. The deformation of plastically non-homogeneous materials. Philos. Mag. 21, 399–424. https://doi.org/10.1080/14786437008238426.

Bayley, C.J., Brekelmans, W.A.M., Geers, M.G.D., 2006. A comparison of dislocation induced back stress formulations in strain gradient crystal plasticity. Int. J. Solid. Struct. 43, 7268–7286. https://doi.org/10.1016/j.ijsolstr.2006.05.011.

Chen, J., Lu, L., Lu, K., 2006. Hardness and strain rate sensitivity of nanocrystalline Cu. Scr. Mater. 54, 1913–1918. https://doi.org/10.1016/j.scriptamat.2006.02.022.
Cottrell, A.H., 1958. Theory of brittle fracture in steel and similar metals. Trans. Met. Soc. AIME 212, 192.
Dalla Torre, F., Lapovok, R., Sandlin, J., Thomson, P.F., Davies, C.H.J., Pereloma, E.V., 2004. Microstructures and properties of copper processed by equal channel angular extrusion for 1–16 passes. Acta Mater. 52, 4819–4832. https://doi.org/10.1016/j.actamat.2004.06.040.
Delincé, M., Bréchet, Y., Embury, J.D., Geers, M.G.D., Jacques, P.J., Pardoen, T., 2007. Structure–property optimization of ultrafine-grained dual-phase steels using a microstructure-based strain hardening model. Acta Mater. 55, 2337–2350. https://doi.org/10.1016/j.actamat.2006.11.029.
Dunstan, D.J., Bushby, A.J., 2014. Grain size dependence of the strength of metals: the Hall–Petch effect does not scale as the inverse square root of grain size. Int. J. Plast. 53, 56–65. https://doi.org/10.1016/j.ijplas.2013.07.004.
Ebrahimi, F., Zhai, Q., Kong, D., 1998. Deformation and fracture of electrodeposited copper. Scr. Mater. 39, 315–321. https://doi.org/10.1016/S1359-6462(98)00164-X.
Eshelby, J.D., Frank, F.C., Nabarro, F.R.N., 1951. XLI. The equilibrium of linear arrays of dislocations. Philos. Mag. Ser. 42, 351–364. https://doi.org/10.1080/14786445108561060.
Estrin, Y., Mecking, H., 1984. A unified phenomenological description of work hardening and creep based on one-parameter models. Acta Metall. 32, 57–70. https://doi.org/10.1016/0001-6160(84)90202-5.
Estrin, Y., Tóth, L.S., Molinari, A., Bréchet, Y., 1998. A dislocation-based model for all hardening stages in large strain deformation. Acta Mater. 46, 5509–5522. https://doi.org/10.1016/S1359-6454(98)00196-7.
Fan, J.T., Ji, X.B., Fu, L.M., Wang, J., Ma, S., Sun, Y.L., Wen, M., Shan, A.D., 2022. Achieving exceptional strength-ductility synergy in a complex-concentrated alloy via architected heterogeneous grains and nano-sized precipitates. Int. J. Plast. 157, 103398 https://doi.org/10.1016/j.ijplas.2022.103398.
Fang, T.H., Li, W.L., Tao, N.R., Lu, K., 2011. Revealing extraordinary intrinsic tensile plasticity in gradient nano-grained copper. Science 331, 1587–1590. https://doi.org/10.1126/science.1200177.
Fu, H.H., Benson, D.J., Meyers, M.A., 2001. Analytical and computational description of effect of grain size on yield stress of metals. Acta Mater. 49, 2567–2582. https://doi.org/10.1016/S1359-6454(01)00062-3.
Gao, H., Huang, Y., Nix, W.D., Hutchinson, J.W., 1999. Mechanism-based strain gradient plasticity-I. Theory. J. Mech. Phys. Solid. 47, 1239–1263. https://doi.org/10.1016/S0022-5096(98)00103-3.
Gao, S., Chen, M., Joshi, M., Shibata, A., Tsuji, N., 2014. Yielding behavior and its effect on uniform elongation in IF steel with various grain sizes. J. Mater. Sci. 49, 6536–6542. https://doi.org/10.1007/s10853-014-8233-0.
Guo, F.J., Wang, Y.F., Wang, M.S., Wei, W., He, Q., Wang, Q.Y., Huang, C.X., Jin, R.R., 2022. The critical grain size for optimal strength–ductility synergy in CrCoNi medium entropy alloy. Scr. Mate. 218, 114808 https://doi.org/10.1016/j.scriptamat.2022.114808.
Hansen, N., 2004. Hall–Petch relation and boundary strengthening. Scr. Mater. 51, 801–806. https://doi.org/10.1016/j.scriptamat.2004.06.002.
Haouala, S., Segurado, J., LLorca, J., 2018. An analysis of the influence of grain size on the strength of FCC polycrystals by means of computational homogenization. Acta Mater 148, 72–85. https://doi.org/10.1016/j.actamat.2018.01.024.
Hazra, S.S., Pereloma, E.V., Gazder, A.A., 2011. Microstructure and mechanical properties after annealing of equal-channel angular pressed interstitial-free steel. Acta Mater. 59, 4015–4029. https://doi.org/10.1016/j.actamat.2011.03.026.
Hirth, J.P., 1972. The influence of grain boundaries on mechanical properties. Metal. Tran. 3, 3047–3067. https://doi.org/10.1007/BF02661312.
Hirth, J.P., Lothe, J., 1982a. Dislocation pileups. Theory of Dislocations. Wiley, New York, pp. 765–790.
Hirth, J.P., Lothe, J., 1982b. Equilibrium of defects concentration. Theory of Dislocations. Wiley, New York, pp. 487–494.
Huang, C.X., Wang, Y.F., Ma, X.L., Yin, S., Höppel, H.W., Göken, M., Wu, X.L., Gao, H.J., Zhu, Y.T., 2018. Interface affected zone for optimal strength and ductility in heterogeneous laminate. Mater. Today 21, 713–719. https://doi.org/10.1016/j.mattod.2018.03.006.
Huang, Y., Qu, S., Hwang, K.C., Li, M., Gao, H., 2004. A conventional theory of mechanism-based strain gradient plasticity. Int. J. Plast. 20, 753–782. https://doi.org/10.1016/j.ijplas.2003.08.002.
Hull, D., Bacon, D.J., 2011. Origin and multiplication of dislocations. Introduction of Dislocations. Elsevier, pp. 157–169.
Hutchinson, J.W., Fleck, N.A., 1997. Strain gradient plasticity. Adv. Appl. Mech. 295–361. https://doi.org/10.1016/S0065-2156(08)70388-0. Elsevier.
Jiang, M.Y., Fan, Z.X., Kruch, S., Devincre, B., 2022. Grain size effect of FCC polycrystal: a new CPFEM approach based on surface geometrically necessary dislocations. Int. J. Plast. 150, 103181 https://doi.org/10.1016/j.ijplas.2021.103181.
Jiang, X.J., Zhang, L.J., Zhang, L., Huang, T.L., Wu, G.L., Huang, X.X., Mishin, O.V., 2019. Heterogeneous microstructure and enhanced mechanical properties in annealed multilayered IF steel. Mater. Sci. Eng. A 759, 262–271. https://doi.org/10.1016/j.msea.2019.05.034.
Kocks, U.F., 1976. Laws for work-hardening and low-temperature creep. J. Eng. Mater. Tech. 98, 76–85.
Lee, S.H., Utsunomiya, H., Sakai, T., 2004. Microstructures and mechanical properties of ultra low carbon interstitial free steel severely deformed by a multi-stack accumulative roll bonding process. Mater. Trans. 45, 2177–2181. https://doi.org/10.2320/matertrans.45.2177.
Li, J.J., Lu, W.J., Chen, S.H., Liu, C.H., 2020. Revealing extra strengthening and strain hardening in heterogeneous two-phase nanostructures. Int. J. Plast. 126, 102626 https://doi.org/10.1016/j.ijplas.2019.11.005.
Li, J.J., Soh, A.K., 2012. Modeling of the plastic deformation of nanostructured materials with grain size gradient. Int. J. Plast. 39, 88–102. https://doi.org/10.1016/j.ijplas.2012.06.004.
Li, J.J., Weng, G.J., Chen, S.H., Wu, X.L., 2017. On strain hardening mechanism in gradient nanostructures. Int. J. Plast. 88, 89–107. https://doi.org/10.1016/j.ijplas.2016.10.003.
Li, S.X., Cui, G.R., 2007. Dependence of strength, elongation, and toughness on grain size in metallic structural materials. J. Appl. Phys. 101, 083525 https://doi.org/10.1063/1.2720184.
Li, X.Y., Lu, K., 2017. Playing with defects in metals. Nat. Mater. 16, 700–701. https://doi.org/10.1038/nmat4929.
Li, Y.S., Zhang, Y., Tao, N.R., Lu, K., 2008. Effect of thermal annealing on mechanical properties of a nanostructured copper prepared by means of dynamic plastic deformation. Scr. Mater. 59, 475–478. https://doi.org/10.1016/j.scriptamat.2008.04.043.
Li, Z., Pradeep, K.G., Deng, Y., Raabe, D., Tasan, C.C., 2016. Metastable high-entropy dual-phase alloys overcome the strength–ductility trade-off. Nature 534, 227–230. https://doi.org/10.1038/nature17981.
Lin, H.R., Tian, Y.Z., Sun, S.J., Zhang, Z.J., Bai, Y., Lu, J.T., Zhang, Z.F., Tsuji, N., 2020. Significant transitions of mechanical properties by changing temperature in Cu-Al alloys with heterogeneous microstructures. Mater. Charact. 168, 110546 https://doi.org/10.1016/j.matchar.2020.110546.
Liu, L.Y., Zhang, Y., Li, J.P., Fan, M.Y., Wang, X.Y., Wu, G.C., Yang, Z.B., Luan, J.H., Jiao, Z.B., Liu, C.T., Liaw, P.K., Zhang, Z.W., 2022a. Enhanced strength-ductility synergy via novel bifunctional nano-precipitates in a high-entropy alloy. Int. J. Plast. 153, 103235 https://doi.org/10.1016/j.ijplas.2022.103235.
Liu, M.W., Gong, W., Zheng, R.X., Li, J., Zhang, Z., Gao, S., Ma, C.L., Tsuji, N., 2022b. Achieving excellent mechanical properties in type 316 stainless steel by tailoring grain size in homogeneously recovered or recrystallized nanostructures. Acta Mater. 226, 117629 https://doi.org/10.1016/j.actamat.2022.117629.
Liu, R., Tian, Y.Z., Zhang, Z.J., Zhang, P., An, X.H., Zhang, Z.F., 2018. Exploring the fatigue strength improvement of Cu-Al alloys. Acta Mater. 144, 613–626. https://doi.org/10.1016/j.actamat.2017.11.019.
Liu, S.S., Xia, D.B., Yang, H., Huang, G.S., Yang, F.X., Chen, X.H., Tang, A.T., Jiang, B., Pan, F.S., 2022c. Mechanical properties and deformation mechanism in Mg-Gd alloy laminate with dual-heterostructure grain size and texture. Int. J. Plast. 157, 103371 https://doi.org/10.1016/j.ijplas.2022.103371.
Liu, X.W., Wu, K., Wu, G., Gao, Y., Zhu, L.L., Lu, Y., Lu, J., 2016. High strength and high ductility copper obtained by topologically controlled planar heterogeneous structures. Scr. Mater. 124, 103–107. https://doi.org/10.1016/j.scriptamat.2016.07.003.
Lu, K., 2014. Making strong nanomaterials ductile with gradients. Science 345, 1455–1456.
Lu, L., Chen, X., Huang, X., Lu, K., 2009. Revealing the maximum strength in nanotwinned copper. Science 323, 607–610. https://doi.org/10.1126/science.1167641.
Ma, X.L., Huang, C.X., Moering, J., Ruppert, M., Höppel, H.W., Göken, M., Narayan, J., Zhu, Y.T., 2016. Mechanical properties of copper/bronze laminates: role of interfaces. Acta Mater. 116, 43–52. https://doi.org/10.1016/j.actamat.2016.06.023.

Ma, X.L., Huang, C.X., Xu, W.Z., Zhou, H., Wu, X.L., Zhu, Y.T., 2015. Strain hardening and ductility in a coarse-grain/nanostructure laminate material. Scr. Mater. 103, 57–60. https://doi.org/10.1016/j.scriptamat.2015.03.006.
Mahajan, S., 1997. Formation of annealing twins in f.c.c. crystals. Acta Mater. 45, 2633–2638. https://doi.org/10.1016/S1359-6454(96)00336-9.
Malygin, G.A., 2007. Plasticity and strength of micro- and nanocrystalline materials. Phys. Solid State 49, 1013–1033. https://doi.org/10.1134/S1063783407060017.
Mazaheri, H., Aval, H.J., Jamaati, R., 2021. Pre-strain assisted low heat-input friction stir processing to achieve ultrafine-grained copper. Mater. Sci. Eng. A 826, 141958. https://doi.org/10.1016/j.msea.2021.141958.
Mecking, H., Kocks, U.F., 1981. Kinetics of flow and strain-hardening. Acta Metall. 29, 1865–1875. https://doi.org/10.1016/0001-6160(81)90112-7.
Meyers, M.A., Chawla, K.K., 2009. Mechanical Behavior of Materials, Second edition. Cambridge University Press.
Meyers, M.A., Mishra, A., Benson, D.J., 2006. Mechanical properties of nanocrystalline materials. Prog. Mater. Sci. 51, 427–556. https://doi.org/10.1016/j.pmatsci.2005.08.003.
Meyersm, M.A., Ashworth, E., 1982. A model for the effect of grain size on the yield stress of metals. Philos. Mag. A 46, 737–759. https://doi.org/10.1080/01418618208236928.
Mitchell, T.E., 1964. The stress-fields around groups of dislocations in face-centred cubic metals. Philos. Mag. 10, 301–314. https://doi.org/10.1080/14786436408225667.
Murr, L.E., 2016. Dislocation ledge sources: dispelling the myth of Frank–Read source importance. Metall. Mater. Trans. A 47, 5811–5826. https://doi.org/10.1007/s11661-015-3286-5.
Murr, L.E., Wang, S.H., 1982. Comparison of microstructural evolution associated with the stress-strain diagrams for nickel and 304 stainless steel: an electron microscope study of microyielding and plastic flow. Res. Mech. 4, 237–274.
Nix, W.D., Gao, H.J., 1998. Indentation size effects in crystalline materials: a law for strain gradient plasticity. J. Mech. Phys. Solid. 46, 411–425. https://doi.org/10.1016/S0022-5096(97)00086-0.
Otto, F., Dlouhý, A., Somsen, C.H., Bei, H., Eggeler, G., George, E.P., 2013. The influences of temperature and microstructure on the tensile properties of a CoCrFeMnNi high-entropy alloy. Acta Mater. 61, 5743–5755. https://doi.org/10.1016/j.actamat.2013.06.018.
Ovid'ko, I.A., Valiev, R.Z., Zhu, Y.T., 2018. Review on superior strength and enhanced ductility of metallic nanomaterials. Prog. Mater. Sci. 94, 462–540. https://doi.org/10.1016/j.pmatsci.2018.02.002.
Pan, Q.S., Zhang, L.X., Feng, R., Lu, Q.H., An, K., Chuang, A.C., Poplawsky, J.D., Liaw, P.K., Lu, L., 2021. Gradient cell–structured high-entropy alloy with exceptional strength and ductility. Science 374, 984–989. https://doi.org/10.1126/science.abj8114.
Purcek, G., Saray, O., Karaman, I., Maier, H.J., 2012. High strength and high ductility of ultrafine-grained, interstitial-free steel produced by ECAE and annealing. Metall. Mater. Trans. A 43, 1884–1894. https://doi.org/10.1007/s11661-011-1063-7.
Ren, C.X., Wang, Q., Hou, J.P., Zhang, Z.J., Zhang, Z.F., Langdon, T.G., 2021. The nature of the maximum microhardness and thickness of the gradient layer in surface-strengthened Cu-Al alloys. Acta Mater. 215, 117073 https://doi.org/10.1016/j.actamat.2021.117073.
Ren, C.X., Wang, Q., Zhang, Z.J., Yang, H.J., Zhang, Z.F., 2018. Surface strengthening behaviors of pure Cu with heterogeneous microstructures. Mater. Sci. Eng. A 727, 192–199. https://doi.org/10.1016/j.msea.2018.05.008.
Ritchie, R.O., 2011. The conflicts between strength and toughness. Nat. Mate. 10, 817–822. https://doi.org/10.1038/nmat3115.
Sanders, P.G., Eastman, J.A., Weertman, J.R., 1997. Elastic and tensile behavior of nanocrystalline copper and palladium. Acta Mater. 45, 4019–4025. https://doi.org/10.1016/S1359-6454(97)00092-X.
Saray, O., Purcek, G., Karaman, I., Neindorf, T., Maier, H.J., 2011. Equal-channel angular sheet extrusion of interstitial-free (IF) steel: microstructural evolution and mechanical properties. Mater. Sci. Eng. A 528, 6573–6583. https://doi.org/10.1016/j.msea.2011.05.014.
Sathiyamoorthi, P., Kim, H.S., 2020. High-entropy alloys with heterogeneous microstructure: processing and mechanical properties. Prog. Mater. Sci., 100709 https://doi.org/10.1016/j.pmatsci.2020.100709.
Sekban, D.M., Saray, O., Aktarer, S.M., Purcek, G., Ma, Z.Y., 2015. Microstructure, mechanical properties and formability of friction stir processed interstitial-free steel. Mater. Sci. Eng. A 642, 57–64. https://doi.org/10.1016/j.msea.2015.06.068.
Sih, G.C., Macdonald, B., 1974. Fracture mechanics applied to engineering problems-strain energy density fracture criterion. Eng. Fract. Mech. 6, 361–386. https://doi.org/10.1016/0013-7944(74)90033-2.
Soboyejo, W.O., 2003. Toughness and fracture process zone. Mechanical Properties of Engineered Materials, Mechanical Engineering. Marcel Dekker, New York, p. 208.
Thompson, A.W., Baskes, M.I., 1973. The influence of grain size on the work hardening of face-center cubic polycrystals. Philos. Mag. 28, 301–308. https://doi.org/10.1080/14786437308217454.
Tian, Y.Z., Zhao, L.J., Park, N., Liu, R., Zhang, P., Zhang, Z.J., Shibata, A., Zhang, Z.F., Tsuji, N., 2016. Revealing the deformation mechanisms of Cu–Al alloys with high strength and good ductility. Acta Mater. 110, 61–72. https://doi.org/10.1016/j.actamat.2016.03.015.
Tsuji, N., Ito, Y., Saito, Y., Minamino, Y., 2002. Strength and ductility of ultrafine grained aluminum and iron produced by ARB and annealing. Scr. Mater. 47, 893–899. https://doi.org/10.1016/S1359-6462(02)00282-8.
Valiev, R.Z., Kozlov, E.V., Ivanov, Y.F., Lian, J., Nazarov, A.A., Baudelet, B., 1994. Deformation behaviour of ultra-fine-grained copper. Acta Metall. Mater. 42, 2467–2475. https://doi.org/10.1016/0956-7151(94)90326-3.
Wang, M.S., Wang, Y.F., He, Q., Wei, W., Guo, F.J., Su, W.L., Huang, C.X., 2022a. A strong and ductile pure titanium. Mater. Sci. Eng. A 833, 142534.
Wang, Y.F., An, J., Yin, K., Wang, M.S., Li, Y.S., Huang, C.X., 2018a. Ultrafine-grained microstructure and improved mechanical behaviors of friction stir welded Cu and Cu–30 Zn Joints. Acta Metall. Sin. (Engl. Lett.) 31, 878–886. https://doi.org/10.1007/s40195-018-0719-3.
Wang, Y.F., Guo, F.J., He, Q., Song, L.Y., Wang, M.S., Huang, A.H., Li, Y.S., Huang, C.X., 2019a. Synergetic deformation-induced extraordinary softening and hardening in gradient copper. Mater. Sci. Eng. A 752, 217–222. https://doi.org/10.1016/j.msea.2019.03.020.
Wang, Y.F., Huang, C.X., Fang, X.T., Höppel, H.W., Göken, M., Zhu, Y.T., 2020. Hetero-deformation induced (HDI) hardening does not increase linearly with strain gradient. Scr. Mater. 174, 19–23. https://doi.org/10.1016/j.scriptamat.2019.08.022.
Wang, Y.F., Huang, C.X., He, Q., Guo, F.J., Wang, M.S., Song, L.Y., Zhu, Y.T., 2019b. Heterostructure induced dispersive shear bands in heterostructured Cu. Scr. Mater. 170, 76–80. https://doi.org/10.1016/j.scriptamat.2019.05.036.
Wang, Y.F., Wang, M.S., Fang, X.T., Guo, F.J., Liu, H.Q., Scattergood, R.O., Huang, C.X., Zhu, Y.T., 2019c. Extra strengthening in a coarse/ultrafine grained laminate: role of gradient interfaces. Int. J. Plast. 123, 196–207. https://doi.org/10.1016/j.ijplas.2019.07.019.
Wang, Y.F., Yang, M.X., Ma, X.L., Wang, M.S., Yin, K., Huang, A.H., Huang, C.X., 2018b. Improved back stress and synergetic strain hardening in coarse-grain/nanostructure laminates. Mater. Sci. Eng. A 727, 113–118. https://doi.org/10.1016/j.msea.2018.04.107.
Wang, Y.F., Zhu, Y.T., Yu, Z.J., Zhao, J.F., Wei, Y.G., 2022b. Hetero-zone boundary affected region: a primary microstructural factor controlling extra work hardening in heterostructure. Acta Mater. 241, 118395 https://doi.org/10.1016/j.actamat.2022.118395.
Wang, Y.M., Chen, M.W., Zhou, F.H., Ma, E., 2002. High tensile ductility in a nanostructured metal. Nature 419, 912–915. https://doi.org/10.1038/nature01133.
Wu, H., Fan, G.H., Huang, M., Geng, L., Cui, X.P., Xie, H.L., 2017. Deformation behavior of brittle/ductile multilayered composites under interface constraint effect. Int. J. Plast. 89, 96–109. https://doi.org/10.1016/j.ijplas.2016.11.005.
Wu, H., Huang, M., Xia, Y., Li, X., Li, R., Liu, C., Gan, W., Xiao, T., Geng, L., Liu, Q., Fan, G., 2022. The importance of interfacial stress-affected zone in evading the strength-ductility trade-off of heterogeneous multi-layered composites. Int. J. Plast. 103485 https://doi.org/10.1016/j.ijplas.2022.103485.
Wu, X.L., Jiang, P., Chen, L., Yuan, F.P., Zhu, Y.T., 2014. Extraordinary strain hardening by gradient structure. Proc. Natl. Acad. Sci. U.S.A. 111, 7197–7201. https://doi.org/10.1073/pnas.1324069111.
Wu, X.L., Yang, M.X., Yuan, F.P., Wu, G.L., Wei, Y.J., Huang, X.X., Zhu, Y.T., 2015. Heterogeneous lamella structure unites ultrafine-grain strength with coarse-grain ductility. Proc. Natl. Acad. Sci. U.S.A. 112, 14501–14505. https://doi.org/10.1073/pnas.1517193112.
Xue, P., Xiao, B.L., Ma, Z.Y., 2012. High tensile ductility via enhanced strain hardening in ultrafine-grained Cu. Mater. Sci. Eng. A 532, 106–110. https://doi.org/10.1016/j.msea.2011.10.070.

Yang, L., Lu, L., 2013. The influence of sample thickness on the tensile properties of pure Cu with different grain sizes. Scr. Mater. 69, 242–245. https://doi.org/10.1016/j.scriptamat.2013.04.009.
Yang, X.C., Ma, X.L., Moering, J., Zhou, H., Wang, W., Gong, Y.L., Tao, J.M., Zhu, Y.T., Zhu, X.K., 2015. Influence of gradient structure volume fraction on the mechanical properties of pure copper. Mater. Sci. Eng. A 645, 280–285. https://doi.org/10.1016/j.msea.2015.08.037.
Yasnikov, I.S., Kaneko, Y., Uchida, M., Vinogradov, A., 2022. The grain size effect on strain hardening and necking instability revisited from the dislocation density evolution approach. Mater. Sci. Eng. A 831, 142330. https://doi.org/10.1016/j.msea.2021.142330.
Yoda, R., Shibata, K., Morimitsu, T., Terada, D., Tsuji, N., 2011. Formability of ultrafine-grained interstitial-free steel fabricated by accumulative roll-bonding and subsequent annealing. Scr. Mater. 65, 175–178. https://doi.org/10.1016/j.scriptamat.2011.02.002.
Yu, C.Y., Kao, P.W., Chang, C.P., 2005. Transition of tensile deformation behaviors in ultrafine-grained aluminum. Acta Mater. 53, 4019–4028. https://doi.org/10.1016/j.actamat.2005.05.005.
Zhao, J.F., Lu, X.C., Yuan, F.P., Kan, Q.H., Qu, S.X., Kang, G.Z., Zhang, X., 2020. Multiple mechanism based constitutive modeling of gradient nanograined material. Int. J. Plast. 125, 314–330. https://doi.org/10.1016/j.ijplas.2019.09.018.
Zhao, Y.H., Bingert, J.F., Liao, X.Z., Cui, B.Z., Han, K., Sergueeva, A.V., Mukherjee, A.K., Valiev, R.Z., Langdon, T.G., Zhu, Y.T., 2006. Simultaneously increasing the ductility and strength of ultra-fine-grained pure copper. Adv. Mater. 18, 2949–2953. https://doi.org/10.1002/adma.200601472.
Zhao, Y.H., Topping, T., Li, Y., Lavernia, E.J., 2011. Strength and ductility of Bi-modal Cu. Adv. Eng. Mater. 13, 865–871. https://doi.org/10.1002/adem.201100019.
Zhong, S.X., Xu, C., Li, Y., Li, W., Luo, H., Peng, R.Z., Jia, X.S., 2022. Hierarchy modification induced exceptional cryogenic strength, ductility and toughness combinations in an asymmetrical-rolled heterogeneous-grained high manganese steel. Int. J. Plast. 154, 103316 https://doi.org/10.1016/j.ijplas.2022.103316.
Zhou, H., Huang, C.X., Sha, X.C., Xiao, L.R., Ma, X.L., Höppel, H.W., Göken, M., Wu, X.L., Ameyama, K., Han, X.D., Zhu, Y.T., 2019. In-situ observation of dislocation dynamics near heterostructured interfaces. Mater. Res. Lett. 7, 376–382. https://doi.org/10.1080/21663831.2019.1616330.
Zhu, Y.T., Ameyama, K., Anderson, P.M., Beyerlein, I.J., Gao, H.J., Kim, H.S., Lavernia, E., Mathaudhu, S., Muhrabi, H., Ritchie, R.O., Tsuji, N., Zhang, X.Y., Wu, X.L., 2021. Heterostructured materials: superior properties from hetero-zone interaction. Mater. Res. Lett. 9, 1–31. https://doi.org/10.1080/21663831.2020.1796836.
Zhu, Y.T., Liao, X.Z., Wu, X.L., 2012. Deformation twinning in nanocrystalline materials. Prog. Mater. Sci. 57, 1–62. https://doi.org/10.1016/j.pmatsci.2011.05.001.
Zhu, Y.T., Wu, X.L., 2019. Perspective on hetero-deformation induced (HDI) hardening and back stress. Mater. Res. Lett. 7, 393–398. https://doi.org/10.1080/21663831.2019.1616331.
Zhu, Y.T., Wu, X.L., 2018. Ductility and plasticity of nanostructured metals: differences and issues. Mater. Today Nano 2, 15–20. https://doi.org/10.1016/j.mtnano.2018.09.004.